# Seasonal and intraseasonal surface chlorophyll-a variability along the northwest African coast

Cyril Lathuilière, Vincent Echevin, Marina Lévy

# Seasonal and intraseasonal surface chlorophyll-a variability along the northwest African coast

C. Lathuilière,[1] V. Echevin,[1] and M. Lévy[1]

Received 3 July 2007; revised 12 October 2007; accepted 31 December 2007; published 7 May 2008.

[1] Five years of SeaWiFS ocean color data are used to characterize the variability of surface chlorophyll (SCHL) over seasonal and intraseasonal timescales along the northwest African coast (between 10°N and 33°N). This variability is interpreted in regards of remotely sensed wind stress and sea surface temperature and of climatological surface nitrate concentration. Three regions with fairly different behaviors are identified: the region of the subtropical gyre (24°N–33°N) is characterized by a weak seasonality and chlorophyll confined at the coast. The inter-gyre region off Cape Blanc (19°N–24°N) is characterized by a weak seasonality and a persistent large offshore extension of chlorophyll. The region of the recirculation gyre (10°N–19°N) is characterized by a strong seasonality and a large offshore extension of chlorophyll from February to May followed by an abrupt chlorophyll drop that propagates northward from May to June. The seasonal variability is well explained by the seasonal variability in wind-forcing. Nutrient limitation is the key factor that explains the weak offshore extension of chlorophyll in the North. The chlorophyll drop in the South is attributed to the weakening of the wind-forcing and the simultaneous advection of warm water from the South by a coastal and seasonal branch of the North Equatorial Counter Current (NECC). Intraseasonal variability is present in all regions. The cases of good correlation between the intraseasonal variability of the chlorophyll and of the wind-forcing are found to be associated with weak chlorophyll offshore extension and large nutrient limitation.

**Citation:** Lathuilière, C., V. Echevin, and M. Lévy (2008), Seasonal and intraseasonal surface chlorophyll-a variability along the northwest African coast, *J. Geophys. Res.*, *113*, C05007, doi:10.1029/2007JC004433.

## 1. Introduction

[2] The northwest African coast is characterized by a strong coastal upwelling [*Wooster et al.*, 1976]. As in other major coastal upwelling systems (Peru-Chili, Benguela and California), this upwelling results from the strong equatorward alongshore component of the trade winds, which drives a cross-shore Ekman transport under the action of the Coriolis force. This offshore transport is compensated by a nearshore upward vertical transport of cold and nutrient-rich waters, which favors phytoplankton growth [*Herbland and Voituriez*, 1974; *Huntsman and Barber*, 1977; *Bricaud et al.*, 1987; *Van Camp et al.*, 1991]. Variability of phytoplankton biomass is expected to be driven by the variability of nutrient inputs, which is related to the variability of the coastal upwelling.

[3] A good indicator of coastal upwelling and of its variability is the Sea Surface Temperature (SST) near the shore. At small timescales, SST cooling events generally occur a few days after upwelling-favorable wind stress events [*Van Camp et al.*, 1991]. Over seasonal and interannual timescales, the link between wind stress and coastal upwelling has also been confirmed, both from historical reports [*Wooster et al.*, 1976] and satellite data [*Van Camp et al.*, 1991; *Nykjaer and Van Camp*, 1994; *Santos et al.*, 2005].

[4] The variability of coastal upwelling results in a strong variability of the forcing of the ecosystem. Comparison of the four major coastal upwelling systems shows that the northwest African coast is the most spatially and seasonally variable one in terms of primary production [*Carr and Kearns*, 2003]. This variability is still poorly documented.

[5] This study has two objectives: First, to document and characterize the variations of SCHL within the Canary upwelling system (10°N–33°N) over seasonal and intraseasonal timescales, with a focus on the cross-shore extension of the high SCHL area. Second, to interpret the observed variability in terms of wind-forcing and to investigate the potential impact of the large scale circulation, with an emphasis on the nutrients variations associated with the large scale circulation.

[6] For this purpose, we used chlorophyll satellite data. Their good spatial and temporal coverage allows the construction of a climatology out of a period without strong interannual event, i.e., 2000–2004; This contrasts with previous studies focusing on the period 1997–1999 characterized by a strong interannual activity [*Thomas et al.*, 2001; *Helmke et al.*, 2005; *Pradhan et al.*, 2006]. In order to interpret the variations of SCHL, wind stress and Sea

[1]LOCEAN/IPSL, UPMC/IRD/CNRS/MNHN, Paris, France.


0148-0227/08/2007JC004433

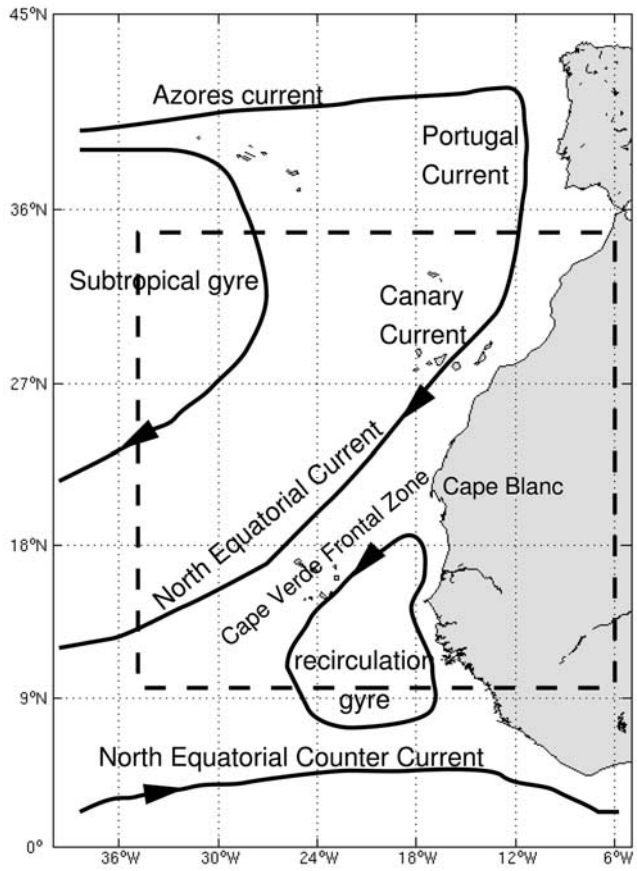


**Figure 1.** Large scale circulation (adapted from *Mittelstaedt* [1991] and *Stramma et al.* [2005]). The study area is superimposed in dashed.

Surface Temperature (SST) remotely sensed products are used as proxies for respectively coastal upwelling forcing and the physical response to coastal upwelling. To complete the description of the biological response, the climatological data set of nitrate is used (see section 3.1).

[7] A description of the large scale circulation is presented in section 2. This drives the distinction of three regions, which have rather different characteristics in terms of chlorophyll variability: the subtropical region (24°N–33°N), the region of the recirculation gyre (10°N–19°N) and, in between, the inter-gyre region off Cape Blanc (19°N–24°N). In section 3 we describe the data sets and in particular how the SCHL climatology is constructed. In section 4, the SCHL seasonal variations are described over the three regions and interpreted in regards of the seasonal variations of the upwelling conditions. The intraseasonal variability of SCHL is presented in section 4.3. The main questions raised by those results are discussed in section 5. First, we provide an explanation for the variations of the offshore extension of the high SCHL concentration zone. Second, we relate the SCHL drop observed in May south of 20°N to the weakening of the trade winds and to the seasonal cycle of the large scale circulation within this region. Finally, we discuss the different behaviors of the response in SCHL to wind-forcing over intraseasonal timescale. A summary of the results is presented in section 6.

## 2. Physical Background

[8] Here we briefly review the circulation in the region (Figure 1). Wind-driven upwelling events occur all along the northwest African coast [*Wooster et al.*, 1976]. The upwelling front between the upwelled cold coastal waters and the warmer open ocean waters is associated with a surface density gradient, geostrophically balanced by an equatorward baroclinic coastal jet [*Allen*, 1973]. The rough estimate of the cold coastal band width is the Rossby radius of deformation [*Allen*, 1973], ranging from 30 km to 60 km in our region of interest [*Chelton et al.*, 1998]. The circulation associated with coastal upwelling is thus confined to the nearshore region. Further offshore, the general circulation is mainly driven by the large-scale wind stress curl. The circulation is dominated by the eastern branch of the north Atlantic subtropical gyre, which consists of the Azores current, the Portugal current, the Canary current and the North Equatorial current (NEC) (Figure 1) [*Barton*, 1998]. North of 22°N, in the subtropical gyre, the large scale circulation along the coast is directed southward. South of 20°N, a cyclonic recirculation gyre drives a predominately poleward circulation along the coast (Figure 1), opposed to the coastal jet [*Mittelstaedt*, 1991]. The recirculation gyre is influenced by the equatorial current system [*Mittelstaedt*, 1991]. Its southern branch is fed by the eastward flowing North Equatorial Counter Current (NECC). The position of this current has a large seasonal cycle [*Mittelstaedt*, 1991; *Stramma et al.*, 2005]. It is located near 5°N in winter and reaches 10°N in the summer. Thus during summer, the NECC is deflected by the coastal boundary and a large part of the flow is directed poleward along the shore. In winter, the NECC flows eastward, south of the African peninsula into the Guinean Gulf. The subtropical gyre and the recirculation gyre are separated by the Cape Verde Frontal zone [*Zenk et al.*, 1991]. At the surface, ocean color images actually show a persistent high-SCHL so-called "giant filament" off Cape Blanc (21°N) [*Van Camp et al.*, 1991; *Gabric et al.*, 1993] associated with the offshore divergence between the subtropical gyre and the recirculation gyre (Figure 1) and confirm results from oceanographic cruises [*Fraga*, 1974; *Mittelstaedt*, 1976].

[9] Moreover in the subtropical gyre, the wind stress curl is negative (Figure 2b), which results in downward Ekman pumping and thus in a deep nutricline (Figure 2b). In the recirculation gyre, the wind stress curl is positive and Ekman pumping is directed upward, resulting in a shallow nutricline. Consequently, there is a large scale meridional gradient in the depth of the nutricline; the nutrient concentration of waters brought by coastal upwelling varies significantly alongshore [*Fraga*, 1974; *Tomczak*, 1981; *Zenk et al.*, 1991; *Barton*, 1998; *Aristegui et al.*, 2004].

## 3. Data and Methods

### 3.1. Data Sets

[10] Three types of satellite-derived products are used: Wind stress, SST and SCHL. This study is restricted to the

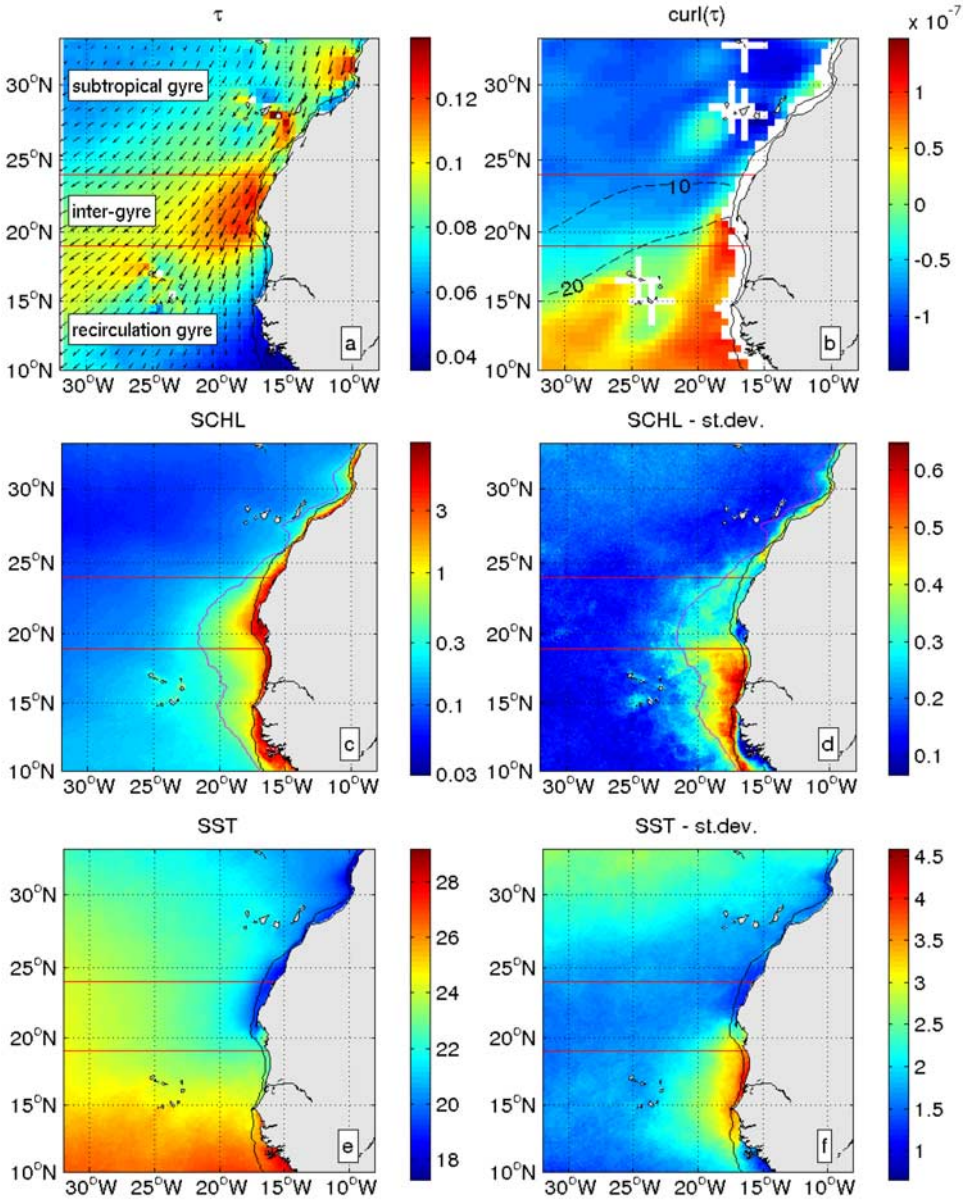


**Figure 2.** Annual mean value over the period 2000–2004 (a) Wind stress (derived from QuikSCAT, resolution 1/2°). (b) Wind stress curl (derived from QuikSCAT, resolution 1/2°) and nitrate concentration at 200 m in black dashed lines (iso-line 10 and 20 mmol/m$^3$). (c) Surface chlorophyll-a (derived from SeaWiFS, resolution 9 km) (mg/m$^3$), the magenta line marks the CEI, which is the line where SCHL is 3 times the offshore SCHL. (d) Standard deviation of log(SCHL). Magenta line is duplicated from c. (e) Sea Surface Temperature (derived from AVHRR, resolution 4 km) (°C). (f) Standard deviation of Sea Surface Temperature (°C). The black line is the shelf break defined by the 200 m isobath. The horizontal red lines mark the latitude of the boundaries of the three regions labeled on Figure (a).

period 2000–2004 which allows to use concomitant SeaWiFS, QuikSCAT and AVHRR data sets. Moreover, this period excludes the strongly anomalous 1998–1999 years following the strong El Nino/La Nina event in the Pacific, which had a significant impact in the Atlantic [*Helmke et al.*, 2005; *Pradhan et al.*, 2006].

[11] We used level 3 (9 km resolution) SeaWiFS data for SCHL. All operations on SCHL are carried out in logarithmic scale in order to respect the lognormal distribution of SCHL [*Campbell*, 1995]. SST estimates are derived from V5 4 km All Sst composite AVHRR (NOAA) data and are associated with a quality index, ranging between 0 and 7. A quality criterion is used in order to remove the artifacts of atmospheric effects: The threshold was chosen at 6 whereas the best sst data set include only sst data with a quality flag of 7 [http://podaac.jpl.nasa.gov:2031/DATA_SET_DOCS/avhrr_pathfinder_sst_v5.html]. Wind stress and wind stress curl products distributed by CERSAT, at IFREMER, Plouzané (France) and based on QuikSCAT sensor, of 1/2° resolution, were also used. Because of this relatively coarse

resolution, the wind stress (curl, respectively) is not available in a narrow coastal band of 50 km, (150 km, respectively) (Figure 2b).

[12] To investigate the seasonal cycle, a climatological year is constructed from the 2000–2004 5-year period for SCHL, SST and wind stress. The climatologies are constructed by averaging 8 day composites for SCHL and SST and 7 day composites for wind stress, and then by smoothing with a window of 20 days and 30 km. To study the intraseasonal variations, daily data were used, which were averaged on a latitudinal band of 1° and smoothed with a 6-day window.

[13] The correlations of anomalies presented in section 4.3 are computed from 8-day SCHL composites and 7-day wind stress composites. The anomalies are calculated by subtracting the mean climatological seasonal cycle. The wind stress anomalies are then regridded on a 8 days temporal grid, with a time lag of 4 days between wind stress and SCHL, which provides the best correlation.

[14] We also used a nitrate climatology from the World Ocean Atlas (WOA, 2001) [http://www.nodc.noaa.gov/OC5/WOA01/pr_woa01.html]. The spatial resolution of these data is 1° and one month.

### 3.2. Derived Indices

[15] We will use three indices for our analysis, which are computed at every latitude and each time step of the climatology:

[16] ● The Cross-Shore Ekman Transport (CSET): CSET = $\tau_{al}/(\rho f)$ with $\tau_{al}$ the equatorward alongshore wind stress, $\rho$ the density and f the Coriolis factor. The CSET is a good index of coastal upwelling because upwelling compensates the cross-shore transport. The wind stress value at approximately 50 km off the shelf break is used, which is the closest good quality wind stress data from the coast. The alongshore component is not the meridional component: we calculated an adjustment for the angle of the coastline.

[17] ● The Temperature-based Upwelling Index (TUI): this index is defined as the difference between the offshore SST (taken as the mean SST in a band located within 500–700 km from the coast) and the SST on the shelf. The TUI measures the impact of upwelling on the SST structure.

[18] ● The Chlorophyll Extension Index (CEI), defined as the distance from the coast where the SCHL concentration is equal to three times the mean SCHL concentration 1200 km–1500 km offshore (Figures 2c and 2d). The CEI measures the lateral extension of the high SCHL band off the coast.

## 4. Results

### 4.1. Mean State and Variability

[19] The SCHL annual mean and standard deviation are shown on Figures 2c and 2d. On annual average, the SCHL distribution shows a sharp contrast between the coastal band and the open ocean (Figure 2c). SCHL values reach more than 1 mg/m$^3$ all along the northwest African coast whereas the mean offshore value is comprised in the range 0.08–0.2 mg/m$^3$. This contrast is clearly the consequence of nutrient upwelling along the coast. The CEI is approximately 50–200 km north of 24°N and increases up to 400 km south of 25°N (magenta line on Figure 2c).

[20] The standard deviation of log(SCHL) shows that the variability of SCHL is mainly restricted to the coastal band limited by the CEI and is low in the open ocean (Figure 2d). Moreover, the standard deviation shows large alongshore variations, with a significant transition at 19°N: it is twice as high in the south compared to the north. Note that, at 12°N and 20°N, the standard deviation is very low close to the coast and higher on the shelf break (Figure 2d). These features can be explained by the topography. In these two locations, the shelf is wide and shallow ensuing in upwelling being localized at the shelf break rather than near the shore [*Estrade*, 2006].

[21] In terms of SST, coastal upwelling induces a nearshore surface cooling because of the deep origin of upwelled waters. Figure 2e, which shows the annual mean SST, clearly reveals this cold coastal band north of 20°N. However, there is no cross-shore SST gradient south of 20°N, which is indicative that another process has to be accounted for. On the other hand, the variability of SST is much higher in the South than in the North (Figure 2f); in the north, the standard deviation of SST at the coast is actually weaker that in the open ocean, whereas in the south, the area of high standard deviation extends up to 500 km from the coast.

[22] It is worth to note that the standard deviation of SCHL (Figure 2d) and SST (Figure 2f) show similar patterns, with a higher variability south of 20°N. This zone corresponds to the cyclonic recirculation gyre (Figure 1) which, as mentioned before, exhibits a strong seasonal variability (section 2).

### 4.2. Seasonal Cycle

[23] Surface chlorophyll variations are now studied on the shelf break along the coast. The climatological seasonal cycle has fairly homogeneous behaviors in the three regions previously defined (Figure 3a):

[24] ● The region of the subtropical gyre (24°N–33°N) is characterized by a small amplitude of the seasonal cycle and a relatively low annual mean SCHL (less than 1 mg/m$^3$).

[25] ● The region of the recirculation gyre (10°N–19°N) is characterized by a large seasonal cycle of SCHL.

[26] ● The inter-gyre region off Cape Blanc (19°N–24°N) is characterized by a small amplitude of the seasonal cycle and a high annual mean SCHL (approximately 2 mg/m$^3$).

[27] ● We will now examine the seasonal cycle in these three regions in details on the basis of Figures 3 and 4.

#### 4.2.1. Region of the Subtropical Gyre

[28] North of 24°N, SCHL displays large alongshore variations (Figure 3a). In particular, two SCHL peaks are noticeable at 27°N and at 31°N, with SCHL values higher than 1 mg/m$^3$, while in between the peaks, SCHL is lower than 0.3 mg/m$^3$. In comparison, temporal variations are relatively weak. They consist mainly in an increase of SCHL in summer at 27°N and 31°N. More precisely, SCHL increases from April to August and decreases from August to October, which is consistent with the seasonal evolution of the upwelling-favorable winds (Figure 3b). Moreover, the CEI remains low, with high chlorophyll concentrations confined to the shelf (less than 30 km from the coast) all yearlong, as shown by a section of SCHL at 26°N (Figure 4a). Note that there is a large variability in the offshore extension of intermediate SCHL values. In summer this distance is approximately 100 km whereas it reaches

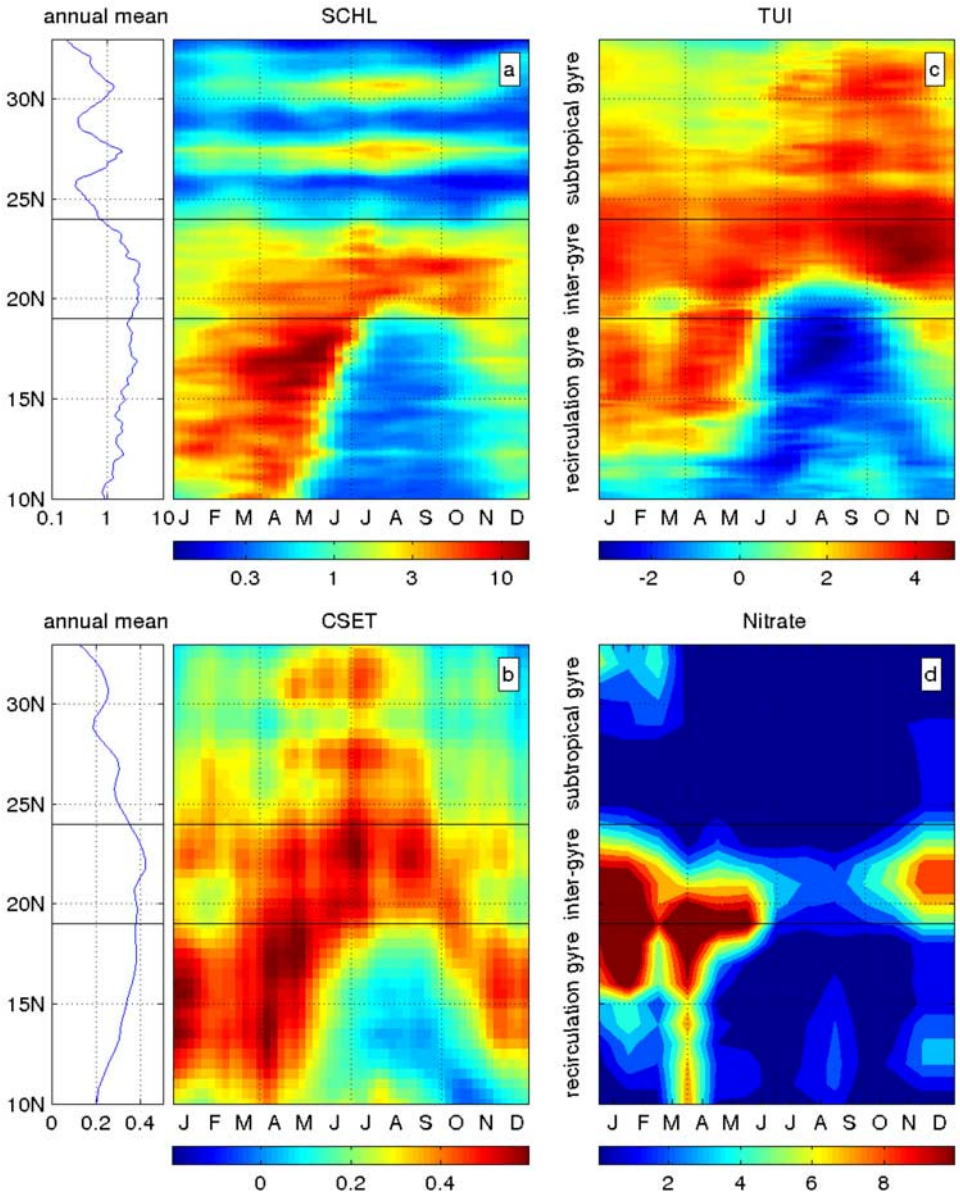


**Figure 3.** Climatological hovmüller along the shore: (a) SCHL on the shelf break (isobath 200 m). The annual mean of SCHL is plotted on the left and the resolution is 9 km and 8 days. (b) CSET ($m^2/s$). The annual mean of CSET is plotted on the left and the resolution is 1/2° and 7 days, (c) TUI, the resolution is 4 km and 8 days. (d) Coastal surface nitrate concentration ($mmole/m^3$) from World Ocean Atlas 2001. The resolution is 1° and 1 month. The horizontal lines mark the boundaries of the region of the subtropical gyre, the inter-gyre region and the region of the recirculation gyre.

400 km in February. The peak of SCHL in winter in the open ocean is characteristic of the winter convection and typical of oligotrophic regimes. The moderate level of maximal SCHL (in comparison with the South, see below) is very likely due to the relatively low nutrient concentration in the subsurface waters, which results from the large scale spatial pattern of the nutricline depth (Figure 2b).

[29] In order to interpret the seasonal variability of SCHL, we now focus on CSET, the upwelling index defined in section 3.2. CSET shows an increase in April and a decrease in August-September (Figure 3b). This CSET peak results from the intensification of the trade winds in Spring and Summer. Latitudinal variations are clearly identified: CSET peaks between 30°N and 33°N and between 26°N and 29°N. These peaks are located off capes, suggesting that orographic effects may accelerate the wind locally (Figure 2a). Previous studies have shown an intensified upwelling off Cape Ghir (31°N) [*Hagen et al.*, 1996; *Pelegri et al.*, 2005] and off Cape Jubi (27°N) interacting with the Canary Islands [*Basterretxea et al.*, 2002; *Barton et al.*, 2004; *Aristegui et al.*, 2004]. The meridional variations of CSET are similar to the SCHL ones, clearly suggesting that the seasonal and latitudinal variability of SCHL north of 24°N is driven by the variability of coastal upwelling. The intensification of CSET in summer results

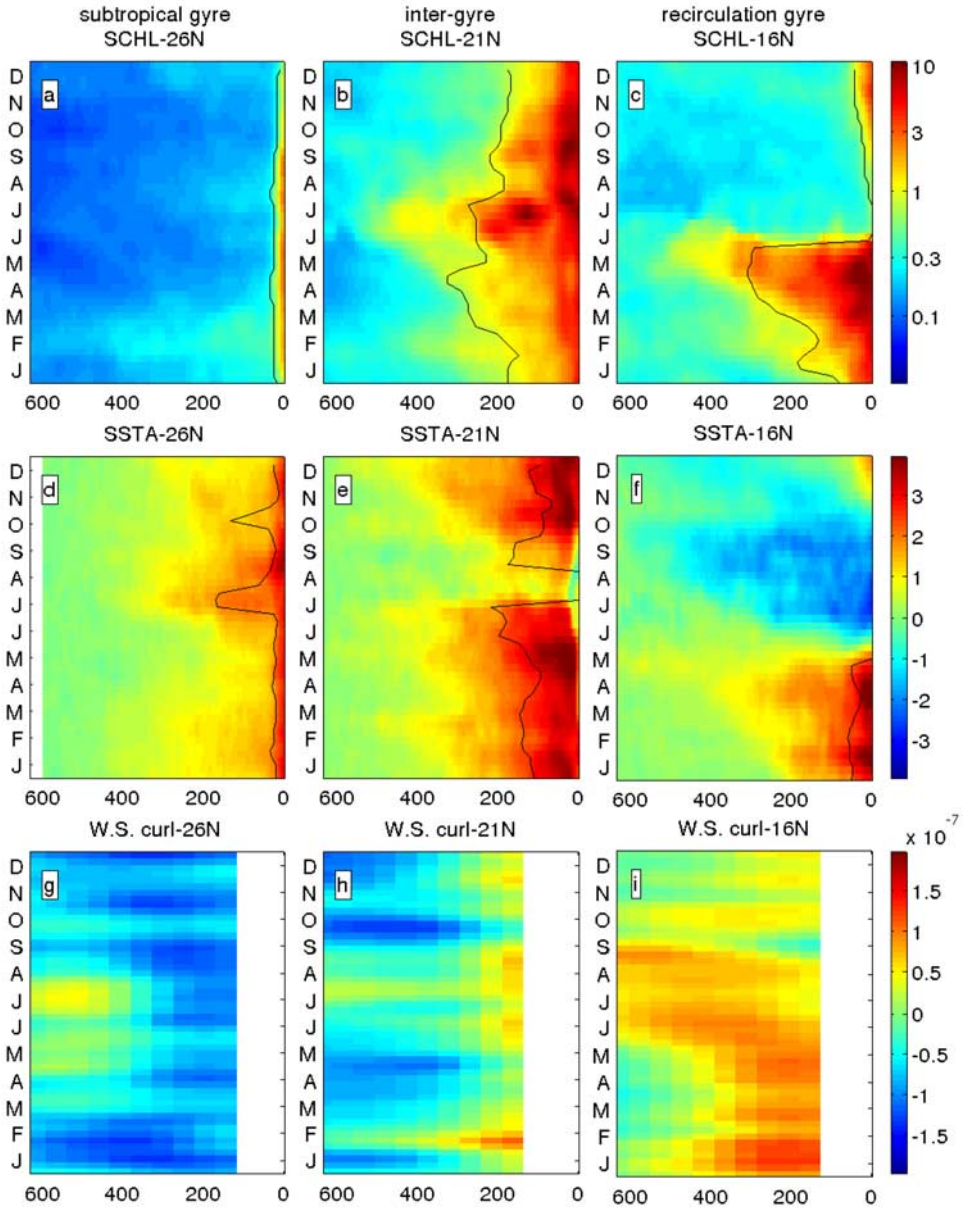


**Figure 4.** Climatological SCHL (resolution 9 km and 8 days), SST anomaly (offshore SST - SST) (resolution 4 km and 8 days) and wind stress curl (resolution 1/2° and 7 days) at 26°N (region of the recirculation gyre), 21°N (inter-gyre region) and 16°N (region of the subtropical gyre). The black lines indicate the position of the CEI (see section 3.2) on (a-c) and the position of the waters 1°C warmer than the coldest waters on (d-f) when the SST coastal anomaly reaches more than 2°C (under upwelling conditions).

in an increase of SCHL. Note that CSET peaks in early July, whereas SCHL peaks in late July early August.

[30] The second upwelling index, related to surface temperature (TUI), gives another perspective on the upwelling conditions. The TUI is persistently positive (Figure 3c), coastal surface waters are thus throughout the year cooler than open ocean surface waters (Figure 2e). Between 27°N and 33°N, the TUI reaches 1°C in winter and increases to more than 3°C from May to September. The rise of TUI is simultaneous with the peak of CSET (Figure 3b) and the peak of SCHL (Figure 3a). Between 24°N and 27°N, the seasonal variability is less pronounced and the TUI remains stable at approximately 3°C.

[31] In brief, the region of the subtropical gyre shows relatively high SCHL peaks at 27°N and 31°N which intensify in spring and decrease in autumn. The variability of these peaks is linked to the variability of the upwelling conditions in space and time. Moreover, the upwelled nutrients are likely to be rapidly consumed by phytoplankton, as shown by the nitrate low surface concentrations all yearlong in this region (Figure 3d).

#### 4.2.2. Region of the Recirculation Gyre

[32] South of 19°N, temporal variations are much stronger than spatial ones. SCHL increases gradually from less than 1 mg/m$^3$ in September to up to 10 mg/m$^3$ in May (Figure 3a). SCHL drops in late Spring, in May at 12°N and

in June at 17°N, exhibiting a northward propagation. A southward propagation of the onset of SCHL increase can also be noticed in October-November south of 19°N. The cross-shore section at 16°N shows that the CEI increases from August to May, reaches up to 400 km in May-June and abruptly drops in June (Figure 4c). By July, the high chlorophyll band has almost disappeared.

[33] The evolution of SCHL is now contrasted with that of CSET (Figure 3b), which is positive and thus favorable to coastal upwelling most of the year. From November to May, the CSET exceeds 0.4 $m^2$/s. In late spring, it progressively decreases to less than 0.2 $m^2$/s. The comparison between SCHL and CSET suggests that high SCHL are closely associated with CSET values higher than 0.2 $m^2$/s. It also confirms that wind-forcing is a key factor in this region. However, note that SCHL is significantly lower in autumn than in winter and spring despite similar CSET values. This suggests that the intensity of the wind-driven upwelling is not the only factor driving seasonal variability. Another factor is likely to be the nitrate concentration (Figure 3d), which is low in autumn and increases during winter. This suggests that the role of the accumulation of nutrients in the surface layer, which are not all assimilated by the ecosystem, may be crucial for the variability.

[34] The TUI also shows a strong seasonal cycle between 12°N and 18°N (Figure 3c). It is positive (3°C) between January and May, drops to a significantly negative value (−2°C) in June, levels off until October and then increases until January. From January to May, positive TUI confirms the occurrence of coastal upwelling (Figure 3b). In summer, negative TUI are observed even though the CSET is positive (Figure 3). This suggests that the SST field is not primarily driven by coastal upwelling during this relaxation period. It is very likely that the warm temperature at the coast (negative TUI) results from the poleward horizontal advection of warm waters by the NECC in summer [*Mittelstaedt*, 1991; *Stramma et al.*, 2005]. The strong seasonality of the TUI, and in particular the fact that coastal waters are actually warmer than offshore waters during part of the year (when TUI < 0), also explains why there is no significant SST gradient south of 20°N between the coast and the open ocean on an annual mean (Figure 2e). As already mentioned for SCHL and CSET, there is a poleward propagation of the TUI drop (Figure 3c). The mechanisms driving this drop will be discussed in section 5.

[35] In summary, the region of the recirculation gyre is characterized by the existence of two well marked seasons: an upwelling season from approximately October to May and a relaxation season from June to September. SCHL gradually increases during the upwelling season, during which the CEI increases. The very high SCHL and the nutrient excess in this region during the upwelling season compared to the northern region, is due to the nutrient richness of subsurface water caused by a shallow nutricline (Figure 2b). A sharp SCHL drop from 10 mg/$m^3$ to 0.3 mg/$m^3$ occurs in May-June. This drop is simultaneous with the decrease of trade winds. Beside, a northward shift in the position of the NECC is also observed at the same time [*Mittelstaedt*, 1991; *Stramma et al.*, 2005]. The relaxation season is marked by low SCHL, low wind-forcing and significantly negative TUI, which suggests advection of water from the South.

#### 4.2.3. Inter-Gyre Region Off Cape Blanc

[36] In the region of transition between the subtropical gyre and the recirculation gyre (19°N–24°N), SCHL is high (>1 mg/$m^3$) all year long (Figure 3a). SCHL is maximum from March to November south of 22°N where it reaches more than 3 mg/$m^3$. Note that this is significantly higher than the maximum in the region of the subtropical gyre. SCHL is lower from December to February. A section of SCHL at 21°N shows a high CEI (Figure 4b). Its width ranges between 200 km and 300 km.

[37] In this region, the CSET is positive throughout the year which is characteristic of persistent upwelling conditions (Figure 3b). A relaxation of the CSET down to 0.2 $m^2$/s can however be noticed from November to February. From February to October, the CSET exceeds 0.4 $m^2$/s. This period corresponds to the period of the highest SCHL. Nitrate concentrations (Figure 3d) are relatively high (more than 3 mmol/$m^3$ from October to June), suggesting that limitation of productivity by nutrients is probably weak. In summer, the nitrate concentration decreases: the ecosystem seems to assimilate a larger part of the upwelled nutrients. Despite this apparently weak limitation by nutrients, SCHL closely follows the CSET temporal variations.

[38] The TUI is positive all year long north of 20°N and from November to May between 19 and 20°N. North of 21°N, the TUI seasonal cycle is similar to the one of the region of the subtropical gyre and is indicative of persistent upwelling conditions. Between 19 and 21°N, the TUI seasonal cycle is more similar to the one of the region of the recirculation gyre, even though CSET is positive even in summer (higher than 0.3 $m^2$/s, Figure 3b).

### 4.3. Intraseasonal Variability

[39] The link between SCHL and wind stress is now studied at intraseasonal timescale. We focus on the region of the subtropical gyre and the region of the recirculation gyre, which show contrasted behaviors. The intraseasonal variability of SCHL is first illustrated by the temporal evolution of SCHL on the shelf break in 2003 (Figure 5). The year 2003 was chosen because of the relatively good coverage of the SeaWiFS data, and we have verified that the other years give qualitatively similar results. Our analyzes focus on two latitudes (16°N and 26°N), which are representative of the region of the subtropical gyre and the region of the recirculation gyre. Then, we compute correlations between SCHL and wind-forcing, based on the 5 years of data and over the entire regions (Figure 6), which allows us to generalize the results presented for 2003.

#### 4.3.1. Region of the Subtropical Gyre

[40] Figure 5a shows the temporal evolution of SCHL and of the equatorward alongshore wind stress during 2003 at 26°N. This evolution is compared to the corresponding climatological seasonal cycle of SCHL and wind stress (dashed lines), which highlights that the variability at intraseasonal timescales has a larger amplitude than the mean seasonal variability.

[41] We focus on the response of SCHL to the wind stress peaks. 13 upwelling events occurred in 2003 (Figure 5a). Most of them ($a_4$, $a_5$, $a_6$, $a_7$, $a_{10}$ and $a_{12}$) are followed by a strong increase in SCHL. In these cases, the time lag

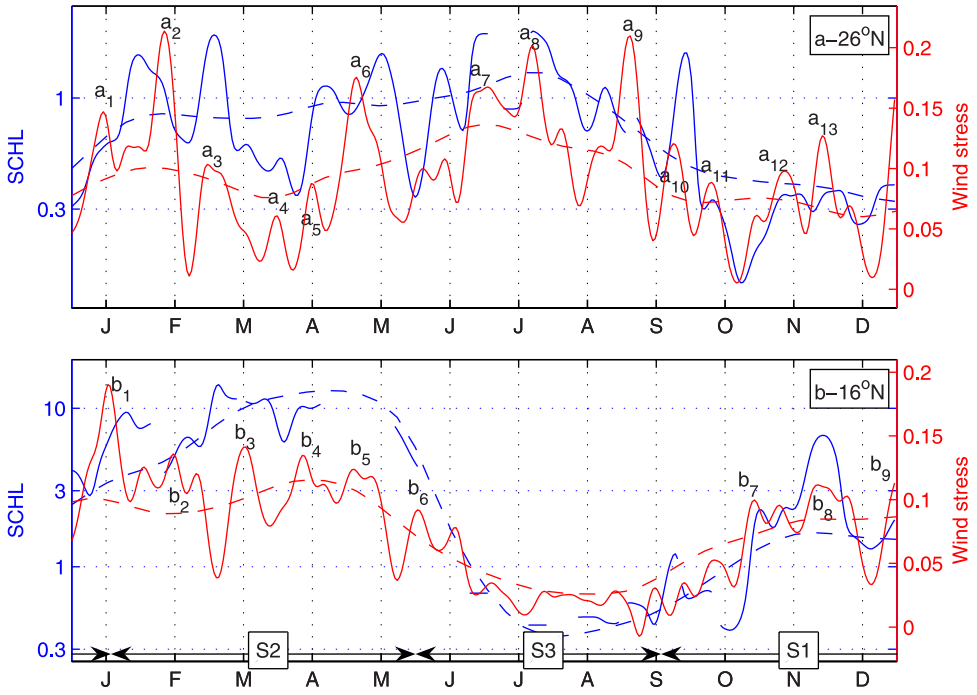


**Figure 5.** Temporal evolution on the shelf break (mean of the 3 pixels nearest the 200 m isobath) of the SCHL (blue) and the southward alongshore wind stress (red) for the year 2003 (solid lines) and the climatological mean seasonal cycle (dashed lines): (a) at 26°N, (b) at 16°N. The temporal resolution is daily but the data are smoothed (see section 3.1).The three defined seasons (see section 4.3.2) are indicated by the arrows: the beginning of the upwelling season (S1), the end of the upwelling season (S2) and the relaxation season (S3).

between the wind stress and the SCHL peak is short and ranges between 0 and 10 days. The remaining wind events provoke different responses of the ecosystem. The peak a1 is followed by a SCHL increase but this increase does not stop after the relaxation of the wind stress. The SCHL maximum occurs more than 15 days after the wind stress peak. Event $a_2$ is unexpectedly followed by a SCHL decrease. Event $a_8$ occurs during a time period with poor SeaWiFS data. High SCHL following event $a_8$ suggests that an increase has occurred during the cloudy period in the beginning of July. Event $a_9$ is not followed by a SCHL peak but the SCHL data coverage was also poor at this time as shown by the gap of the solid blue line. Events $a_4$, $a_{11}$ and $a_{13}$ are followed by a weak SCHL peak. In brief, the SCHL variability is in most cases well explained by the wind stress variability. Only a few events ($a_2$ and possibly $a_9$) fall out of that rule.

#### 4.3.2. Region of the Recirculation Gyre

[42] In the southern region, the SCHL intraseasonal variability has a smaller amplitude than the seasonal cycle (Figure 5b). To better characterize the description of the variability in this region, we distinguish 3 seasons

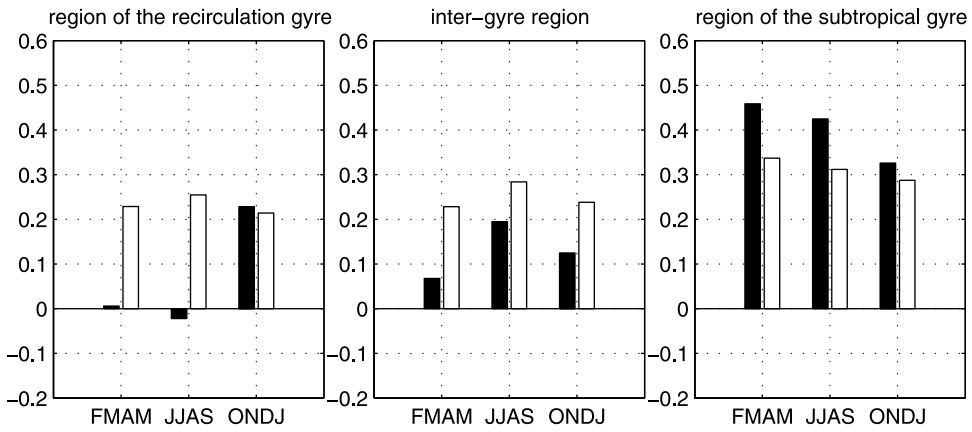


**Figure 6.** Mean correlation between equatorward alongshore wind stress anomalies and SCHL anomalies (black bars) over the period 2000–2004. The significance threshold with a confidence of 95% is indicated by the white bars.

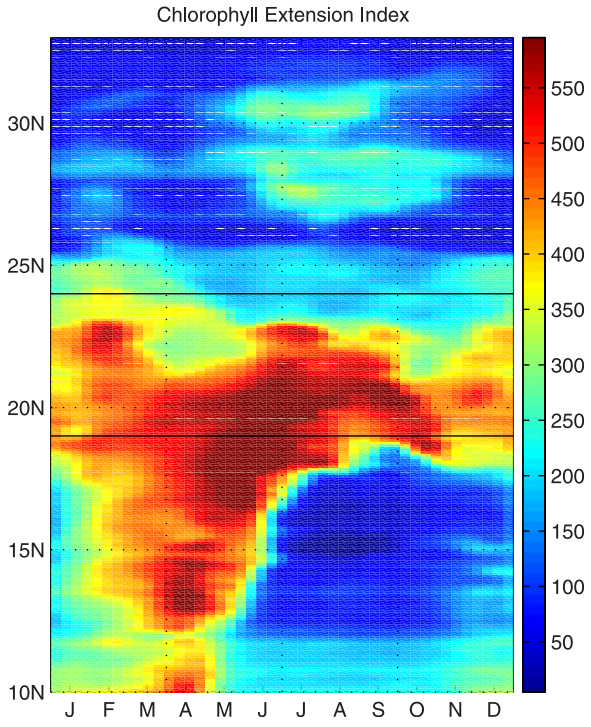


**Figure 7.** CEI (definition in section 3.2) computed from the SeaWiFS climatology. The resolution is 9 km and 8 days.

(Figure 5b): the beginning of upwelling season (September-January), the end of the upwelling season (February-May) and the relaxation season (May-September). Note that these seasons are illustrated by the arrows on Figure 5b.

[43] At the beginning of the upwelling season (from September to January), wind stress conditions become favorable to upwelling. Once equatorward alongshore wind stress reaches 0.05 $m^2/s$ (event $b_7$) SCHL increases from 0.4 $mg/m^3$ to more than 2 $mg/m^3$. From November to January, SCHL peaks follow the wind stress peaks: $b_7$, $b_8$, $b_9$, $b_1$ are followed by SCHL maximum with a short time lag (between 0 and 5 day), which is similar to what happens in the region of the subtropical gyre. On the opposite, from February to May, peaks of wind stress ($b_2$, $b_3$, $b_4$) are not followed by SCHL peaks. The variations of SCHL do not seem to be related with those of the wind stress. From April to June, the response in SCHL is not detected by the satellite because of the high cloud coverage associated with the African monsoon. Responses to events $b_5$ and $b_6$ are thus missing. Wind stress variations show a slight relaxation in March (between $b_2$ and $b_3$). However, SCHL increases at the same time. From May to August, during the highly cloudy relaxation season associated with the African monsoon, SCHL data are sparse, and the SCHL values are weak (approximately 0.5 $mg/m^3$), which makes it difficult to relate its variations with those of wind stress.

#### 4.3.3. Correlations

[44] A quantification of the link between wind stress and SCHL, based on 5 years of data, is given by the correlation of wind stress anomalies and SCHL anomalies (Figure 6). Details are given in section 3.1. In the region of the recirculation gyre, the correlation is significant only during the third season (October to January) and relatively weak (0.25), which confirms the qualitative results. In the inter-gyre region, no significant correlation is found. In the region of the subtropical gyre, the correlation between wind stress and SCHL anomalies is significant all yearlong and is relatively high, strongest in Spring with a value of 0.45.

[45] In summary, the link between the intraseasonal variability of SCHL and the intraseasonal variability of the wind-forcing, namely the occurrence of synoptic events, remains strong throughout the year in the North, whereas it is significant only at the beginning of the upwelling season in the South. The processes, which may explain the relations between the wind stress and the biological response will be discussed in the next section.

## 5. Discussion

[46] This study has investigated the variability of surface chlorophyll variability along the NW African coast over seasonal and intraseasonal timescales and how it relates to the variability of the wind. We now focus on three issues: first, we seek to understand what drives the variations of the CEI. Second, we address the cause of the drop of SCHL in late Spring in the region of the recirculation gyre. Third, we investigate why the link between the wind-forcing and the SCHL concentration at intraseasonal timescales fluctuates over the seasons.

### 5.1. Offshore Extension of Chlorophyll

[47] Our results highlight that the CEI is highly variable in time and in space. Figure 7 shows that the CEI remains narrow (less than approximately 100 km) in the region of the subtropical gyre, wide (approximately 200 km) in the inter-gyre region and its width steeply fluctuates between less than 10 km during the relaxation season and approximately 400 km at the end of the upwelling season in the region of the recirculation gyre. Furthermore, the seasonal variations of this index in the region of the recirculation gyre are well explained by the seasonal cycle of the wind-forcing (Figures 3b and 7). We now focus on the meridional variations. Here we discuss the potential impact of several processes, physical and biological: the distance of the upwelling front from the coast, the wind stress curl, the mesoscale and submesoscale dynamics, and the limitation of phytoplankton growth by nutrients.

[48] Let us first consider the physical processes. The first dynamical characteristic which impacts the CEI is the distance of the upwelling front from the coast. Within this band, cold nutrient-rich waters upwell and phytoplanktonic biomass is produced. The front which separates the cold recently upwelled waters from the open ocean waters, is, according to theoretical studies, roughly located at a distance of one Rossby radius of deformation ($R_d$) [*Allen*, 1973]. In our region, the alongshore variation of the Coriolis parameter and of the stratification induces significant variations of $R_d$. Estimations based on climatological data show a poleward decrease of $R_d$ [*Chelton et al.*, 1998]: $R_d$ is approximately 60 km at 15°N, 40 km at 21°N and 30 km north of 27°N. We now compare those theoretical values to the width of the cold coastal band, defined as the area where SST is within 1°C of the coldest upwelled waters (Figures 4d, 4e and 4f). The width of this coastal band varies significantly with latitude. In the south it can be

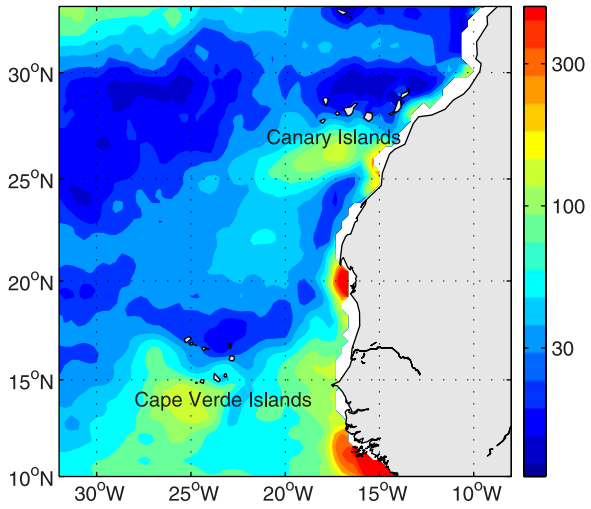


**Figure 8.** Eddy kinetic energy ($cm^2/s^2$) estimated from geostrophic velocities derived from satellite-derived sea level anomalies.

estimated to 40 km during the upwelling season (Figure 4f). Off Cape Blanc (21°N) it reaches 80 km (Figure 4e) and it drops to less than 30 km at 26°N (Figure 4d). This shows a good agreement between the theoretical estimations and the observations except at 21°N, where the large scale circulation results in an offshore divergence off Cape Blanc. Thus from north to south, the upwelling and the primary production occur in a wider coastal band, and chlorophyll-rich waters are less confined to the coast.

[49] The second process is the impact of upward Ekman pumping associated with positive wind stress curl on nutrient input. An important contribution of Ekman pumping in a band extending 200 km from the coast has been reported in several regions where coastal upwelling occurs [*Enriquez and Friehe*, 1995; *Castelao and Barth*, 2006]. The vertical mass flux due to Ekman pumping in this coastal band can reach the same magnitude as the vertical nearshore upward mass flux due to coastal upwelling, as was shown for instance along the Brazilian coast [*Castelao and Barth*, 2006]. In order to evaluate the impact of this process over seasonal timescale, we now compare climatological wind stress curl section at 16°N, 21°N and 26°N to SCHL section (Figures 4g-4i). Note that the wind stress curl products used in this study do not provide data within a 150 km wide coastal band. Assuming that wind stress curl patterns are continuous and that the coast tends to create positive wind stress curl [*Bakun and Nelson*, 1991; *Capet et al.*, 2004], wind stress curl can be extrapolated in the masked coastal band, based on the data between 100 km and 200 km from the coast. In the region of the recirculation gyre, positive wind stress curl extends to 300 km from shore between January and September (Figure 4i). Ekman pumping may thus enhance primary production during the upwelling season. However, the period of positive wind stress curl continues beyond May, when the abrupt SCHL drop occurs. This suggests that SCHL is not significantly affected by the nutrient input by Ekman pumping over seasonal timescale, although it has been shown to contribute to half of the variance of the anomalies of SCHL on interannual timescale [*Pradhan et al.*, 2006].

[50] Mesoscale dynamics, such as for instance advection by filaments, has been shown to be a major process in the cross shelf particle transport off the Cape Blanc region [*Karakas et al.*, 2006]. Between 17°N and 23°N, *Kostianoy and Zatsepin* [1996] estimated that half of the upwelled waters flow across the upwelling front in filaments. To investigate the possible role of mesoscale dynamics, we examine the alongshore variations of eddy kinetic energy, assuming that strong mesoscale and submesoscale activity result in a high eddy kinetic energy (EKE) in our region. EKE is estimated from sea level anomalies from the merged mapped product AVISO using measures of Topex-Poseidon and ERS during the period 1992–2005 [http://www.jason.oceanobs.com/html/donnees/produits/hauteurs/global/msla_fr.html]. Geostrophic velocities anomalies are deduced from sea level anomalies and a 3-month high-pass filter is applied to subtract the seasonal and interannual variability. Figure 8 displays the patterns of EKE. It is high downwind of the Canary and Cape Verde archipelagos and in the coastal zone especially south of 17°N. Progressing south, EKE clearly increases alongshore from 50 $cm^2/s^2$ (17°N) to 100 $cm^2/s^2$ (12°N–15°N). The CEI width may thus increase southward due to an increase of the horizontal mixing induced by mesoscale processes. Note that the nature of the mesoscale processes involved can be various, as for instance mesoscale eddies, baroclinic instabilities of the upwelling jet, coastal and planetary waves and that mesoscale dynamics and wind stress are interlinked and cannot be considered as two separate processes.

[51] In addition to physical processes, the impact of the limitation of phytoplankton growth by nutrients may be a crucial process. When nutrients limit phytoplankton growth, they are quickly consumed and their surface concentration is generally low. When nutrients are not limiting the growth, they are only partly consumed near the shore. The remaining nutrients are advected offshore by Ekman transport, allowing phytoplankton to grow offshore, in a large coastal band. We hypothesize that the offshore extension of SCHL occurs when the nutrient input from the deep water is larger than the uptake by phytoplankton growth at the coast. In order to test this hypothesis, we examine the climatological nutrient distribution. Surface nitrate concentration is low in the region of the subtropical gyre, less than 1 $mmol/m^3$ (Figure 3d). It is more than 5 $mmol/m^3$ most of the year in the inter-gyre region, with a slight minimum in summer at 2 $mmol/m^3$. In the region of the recirculation gyre, it is systematically low (less than 1 $mmol/m^3$) during the relaxation season (May-October) and increases from November to March. Note that this nitrate increase is simultaneous with the increase of SCHL and the increase of the CEI. To further support this biological hypothesis, we also notice that, as mentioned in section 2, the reversal of the wind stress curl around 20°N results in more nutrients in the south than in the north. This is apparent in the subsurface NO3 distribution (Figure 2b) and PO4 distribution in the upwelled waters [*Carr and Kearns*, 2003, Figure 2]. Since the annual mean vertical mass flux, estimated in this study by the CSET, is roughly spatially constant (0.2–0.4 $m^2/s$, Figure 3b), the meridional variations

of the annual coastal nutrient input is thus primarily driven by the meridional variations of the nutrient concentration in the source waters, which are then upwelled. Consequently, the coastal nutrient input is much stronger in the South and this vertical flux of nutrients exceeds the assimilation capacity of the ecosystem.

### 5.2. Dual Cause of the Chlorophyll Drop

[52] Our results have pointed out a sharp drop of SCHL in May in the region of the recirculation gyre. This drop is concomitant with the weakening of wind-forcing (Figures 3a and 3b), which is surprisingly moderate. The weakening of the CSET begins one month before SCHL begins to decrease. This is not surprising since the excess of nutrient in April (Figure 3d) can sustain phytoplankton growth after the upwelling season. A particularly noticeable characteristic of the SCHL drop is its northward propagation with time. A northward propagation of the signal in CSET is also observed (Figure 3b). It is very likely that, the weakening of the wind-forcing is not sufficient to explain the SCHL drop, since a CSET value of 0.2 $m^2/s$ is sufficient to trigger an increase of SCHL up to 1 $mg/m^3$ in October but not sufficient to maintain more than 0.3 $mg/m^3$ in June (Figure 3). Another process has to be accounted for: the advection of chlorophyll-poor water by the NECC during this season. This hypothesis is suggested by the equatorial current system. In spring, the coastal circulation is oriented poleward in the region of the recirculation gyre (especially due to NECC). The advection of warm waters is also consistent with the highly negative TUI value observed in summer south of 20°N (Figure 3c). This advection from the South also results in transport of nutrient- and chlorophyll-poor waters originating offshore in the South. Figure 3a shows that the SCHL (and CSET) drop propagates at 10/15 km/day (11/17 cm/s). This is consistent with the velocity of the NECC, which further support the hypothesis of the advection by the NECC. Note that the two processes, the weakening of the trade winds and the advection by the NECC, are very likely coupled.

### 5.3. Intraseasonal Variability

[53] Our results have highlighted two different behaviors in terms of the response of SCHL to wind stress over intraseasonal timescale. First, the one expected in cases of nutrient limitation: a few days (5–10 days) after a wind-forcing peak, a peak of SCHL is observed. Note that this time lag is also consistent with the time lags deduced from observations in the California current system [*Spitz et al.*, 2005]. This expected behavior is observed all year long in the North and at the beginning of the upwelling season is the South, where, as mentioned in section 5.1, phytoplankton growth is limited by nutrients. Thus the intraseasonal variability of SCHL is to a large extent driven by the intraseasonal variability of the nutrient input, which closely depends on the intraseasonal variability of coastal upwelling.

[54] A different behavior is observed in the South at the end of the upwelling season. In that case there is no correlation between the SCHL variations and the wind-forcing variations. During this season, the nitrate surface concentration is quite high (Figure 3d), indicating that the limitation by nutrient is weak (section 5.1). A new input of nutrients by an upwelling-favorable wind event does not trigger an immediate response of the ecosystem.

[55] Even though our interpretation is well supported by the surface nitrate concentrations, other processes might affect the intraseasonal variability of SCHL and explain the absence of correlation between SCHL and wind stress, such as rapid grazing and propagation of coastal trapped waves. By deflecting the nutricline downward and upward, coastal trapped waves may induce a variability in the coastal nutrient input. However, a close examination of the sea level anomaly time series does not reveal significant propagation events at this latitude and at the time period of decorrelation (not shown). Moreover the sea level anomaly over intra seasonal timescale are rather forced by the local wind-forcing north of 12°N than the result of a wave propagation [*Lazar et al.*, 2006].

## 6. Summary

[56] In this study, satellite and climatological data were used to investigate the variability of SCHL along the northwest African coast over seasonal and intraseasonal timescales. The SCHL variations are compared to those of the wind-forcing, the main driving force of the coastal upwelling. Previous studies, based on snapshot ocean color images and on oceanographic cruises, have suggested the existence of a significant spatial and temporal variability of the offshore extension of high surface chlorophyll concentrations. This study provides a basin-wide description of the seasonal SCHL patterns, that confirms spatially and temporally localized observations. Our approach also permits the assessment of this extension over seasonal timescale. This new outcome has been allowed by the good coverage of the ocean color images and the existence of long time series. This study emphasizes strong variations along the coast and has delimited three regions with fairly different behaviors: the region of the subtropical gyre (24°N–33°N), the inter-gyre region off Cape Blanc (19°N–24°N) and the region of the recirculation gyre (10°N–19°N).

[57] The region of the subtropical gyre is characterized by a weak SCHL seasonal cycle peaking in summer with relatively low SCHL values. Upwelling conditions are persistent all yearlong but the high chlorophyll is confined to the shelf. The negative wind stress curl deflects the nitracline downward, resulting in a lower nutrient concentration in the upwelled waters than further South. During upwelling events, the upwelled nutrients are rapidly consumed near the shore: the offshore extension of SCHL is thus weak and the intraseasonal variability of SCHL immediately responds to that of the wind stress.

[58] The region of the recirculation gyre is characterized by a strong seasonal cycle with an upwelling season from October to May and a relaxation season between June and September. The concentration of SCHL and its offshore extension gradually increase during the upwelling season and abruptly drop in May. The amplitude of the intraseasonal variability is low compared to the amplitude of the seasonal cycle. This region is characterized by a positive wind stress curl, which deflects the nitracline upward, increasing the nutrient concentration in the subsurface waters. At the beginning of the upwelling season, the response in SCHL to intraseasonal wind variations is similar to that of the region of the subtropical gyre. During the later period of the upwelling season, the variations of SCHL

concentration are not related to the variations of the wind stress. This unexpected response in SCHL is likely caused by the weakening of the nutrient limitation of phytoplankton growth, due to the high nutrient surface concentration in this time period. An excess of nutrients also appears as the major process allowing chlorophyll-rich waters to extend offshore, although mesoscale dynamics may also contribute to this offshore extension.

[59] Our results show an abrupt drop of SCHL at the end of the upwelling season, which propagates northward from 10°N to 20°N. Contrasting wind and SST climatologies suggests that this drop results from the simultaneous decrease of the wind-driven upwelling and from the advection of warm and chlorophyll-poor waters from the South by the coastal branch of the NECC.

[60] The main limitation of our approach is that it is based only on the variability of phytoplankton. Information on the distribution of zooplankton would allow a more accurate description of the biological processes. The fluxes between the different components of the ecosystem may also be crucial to advance the understanding of the offshore extension of the rich ecosystem associated with coastal upwelling. Moreover, the spatial and temporal coverage of satellite data limits the description of the intraseasonal variability of the chlorophyll. To further investigate the mechanisms driving the observed chlorophyll distribution, future work will use a coupled biophysical model on the basis of the accurate description of the mean seasonal variability of the surface chlorophyll, which is the main outcome of this study.

[61] **Acknowledgments.** The work of Cyril Lathuilière was supported by DGA. Financial support for this research was also provided by CNRS, IRD, CNES and MERCATOR.

## References

Allen, J. S. (1973), Upwelling and coastal jets in a continuously stratified ocean, *J. Phys. Oceanogr.*, *3*(3), 245–257.

Aristegui, J., X. A. Alvarez-Salgado, E. D. Barton, F. G. Figueiras, S. Hernandez-Leon, C. Roy, and A. M. P. Santos (2004), Oceanography and fisheries of the Canary current/Iberian region of the eastern North Atlantic, in *The Sea*, chap. 23, vol. 14, edited by A. R. Robinson and K. H. Brink, pp. 877–931, John Wiley and Sons, Inc., New York.

Bakun, A., and C. Nelson (1991), The seasonal cycle of wind-stress curl in subtropical eastern boundary current regions, *J. Phys. Oceanogr.*, *21*, 1815–1834.

Barton, E. D. (1998), Eastern boundary of the north atlantic: Northwest Africa and Iberia, in *The Sea*, vol. 11, edited by A. R. Robinson and K. H. Brink, pp. 633–657, John Wiley and Sons, Inc., New York.

Barton, E. D., J. Aristegui, P. Tett, and E. Navarro-Pérez (2004), Variability in the Canary Islands area of the filament-eddy exchanges, *Prog. Oceanogr.*, *62*, 71–94.

Basterretxea, G., E. D. Barton, P. Tett, P. Sangra, E. Navarro-Perez, and J. Aristegui (2002), Eddy and deep chlorophyll maximum response to wind-shear in the lee of Gran Canaria, *Deep Sea Res., Part I*, *49*, 1087–1101.

Bricaud, A., A. Morel, and J.-M. André (1987), Spatial/temporal variability of algal biomass in the mauritanian upwelling zone, as estimated from CZCS data, *Adv. Space Res.*, *7*(2), 53–62.

Campbell, J. (1995), The lognormal distribution as a model for bio-optical variability in the sea, *J. Geophys. Res.*, *100*(C7), 13,237–13,254.

Capet, X. J., P. Marchesiello, and J. C. McWilliams (2004), Upwelling response to coastal wind profiles, *Geophys. Res. Lett.*, *31*, L13311, doi:10.1029/2004GL020123.

Carr, M.-E., and E. Kearns (2003), Production regimes in four eastern boundary current systems, *Deep Sea Res., Part II*, *50*, 3199–3221.

Castelao, R., and J. Barth (2006), Upwelling around cabo Frio, Brazil: The importance of wind stress curl, *Geophys. Res. Lett.*, *33*, L03602, doi:10.1029/2005GL025182.

Chelton, D. B., R. A. deSzoeke, M. G. Schlax, K. El Naggar, and N. Siwertz (1998), Geographical variability of the first baroclinic Rossby Radius of deformation, *J. Phys. Oceanogr.*, *28*, 433–460.

Enriquez, A., and C. Friehe (1995), Effects of wind stress and wind stress curl variability on coastal upwelling, *J. Phys. Oceanogr.*, *25*, 1651–1671.

Estrade, P. (2006), Wide and shallow shelf response to wind-driven upwelling. Application to the Canary Current system, Phd thesis, Université de Bretagne Occidentale, Brest, France.

Fraga, F. (1974), Distribution des masses d'eau dans l'upwelling de Mauritanie, *Tethys*, *6*(1–2), 5–10.

Gabric, A., L. Garcia, L. Van Camp, L. Nykjaer, W. Eifler, and W. Schrimpf (1993), Offshore export of shelf production in the cape blanc (Mauritania) giant filament as derived from coastal zone color scanner imagery, *J. Geophys. Res.*, *98*(C3), 4697–4712.

Hagen, E., C. Zülicke, and R. Feistel (1996), Near-surface structures in the Cape Ghir filament off Morocco, *Oceanol. Acta*, *19*, 6577–6598.

Helmke, P., O. Romero, and G. Fischer (2005), Northwest African upwelling and its effect on offshore organic carbon export to the deep sea, *Global Biogeochem. Cycles*, *19*, GB4015, doi:10.1029/2004GB002265.

Herbland, A., and B. Voituriez (1974), La production primaire dans l'upwelling mauritanien en mars 1973, *Cah. O.R.S.T.O.M., sér. Océanogr.*, *12*(3), 187–201.

Huntsman, S. A., and R. T. Barber (1977), Primary production off northwest Africa: The relationship to wind and nutrient conditions, *Deep Sea Res.*, *24*, 25–33.

Karakas, G., N. Nowald, M. Blaas, P. Marchesiello, S. Frickenhaus, and R. Schlitzer (2006), High-resolution modelling of sediment erosion and particule transport across the northwest African shelf, *J. Geophys. Res.*, *111*, C06025, doi:10.1029/2005JC003296.

Kostianoy, A. G., and A. G. Zatsepin (1996), The West African coastal upwelling filaments and cross-frontal water exchange conditioned by them, *J. Mar. Syst.*, *7*, 349–359.

Lazar, A., I. Polo, S. Arnault, and G. Mainsant (2006), Kelvin waves activity in the eastern tropical Atlantic, Proceedings of the Symposium on 15 Years of Progress in Radar Altimetry. March 13-18, 2006. Venice, Italy (ESA SP-614, July 2006).

Mittelstaedt, E. (1976), On the currents along the Northwest African coast south of 22° North, *Dt. hydrogr. Z.*, *29*(3), 97–117.

Mittelstaedt, E. (1991), The ocean boundary along the northwest African coast: Circulation and oceanographic properties at the sea surface, *Prog. Oceanogr.*, *26*, 307–355.

Nykjaer, L., and L. Van Camp (1994), Seasonal and interannual variability of coastal upwelling along northwest Africa and Portugal from 1981 to 1991, *J. Geophys. Res.*, *99*(C7), 14,197–14,207.

Pelegri, J. L., et al. (2005), Hydrographic cruises off northwest Africa: The Canary current and the Cape Ghir region, *J. Mar. Syst.*, *54*, 39–63.

Pradhan, Y., S. L. Lavender, N. J. Hardman-Mountford, and J. Aiken (2006), Seasonal and inter-annual variability of chlorophyll-a concentration in the Mauritanian upwelling: Observation of an anomalous event during 1998–1999, *Deep Sea Res., Part II*, *53*, 1548–1559.

Santos, M. P., A. S. Kazmin, and A. Peliz (2005), Decadal changes in the Canary upwelling system as revealed by satellite observations: Their impact on productivity, *J. Mar. Res.*, *63*, 359–379.

Spitz, Y. H., J. S. Allen, and J. Gan (2005), Modeling of ecosystem processes on the Oregon shelf during the 2001 summer upwelling, *J. Geophys. Res.*, *110*, C10S17, doi:10.1029/2005JC002870.

Stramma, L., S. Hüttl, and J. Schafstall (2005), Water masses and currents in the upper tropical northeast Atlantic off northwest Africa, *J. Geophys. Res.*, *110*, C12006, doi:10.1029/2005JC002939.

Thomas, A. C., M.-E. Carr, and P. T. Strub (2001), Chlorophyll variability in eastern boundary currents, *Geophys. Res. Lett.*, *28*(18), 3421–3424.

Tomczak, M., Jr. (1981), An analysis of mixing in the frontal zone of south and north Atlantic central water off north-west Africa, *Prog.*, 10,173–10,192.

Van Camp, L., L. Nykjaer, E. Mittelstaedt, and P. Schlittenhardt (1991), Upwelling and boundary circulation off northwest Africa as depicted by infrared and visible satellite observations, *Prog. Oceanogr.*, *26*, 357–402.

Wooster, W., A. Bakun, and D. McLain (1976), The seasonal upwelling cycle along the eastern boundary of the north Atlantic, *J. Mar. Res.*, *34*, 131–141.

Zenk, W., B. Klein, and M. Schröder (1991), Cape Verde frontal zone, *Deep Sea Res., Part I*, *38*, S505–S530.

V. Echevin, C. Lathuilière, and M. Lévy, LOCEAN/IPSL, Université Pierre et Marie Curie, 4 pl. Jussieu, F-75252 Paris Cedex 05, France. (vincent.echevin@locean-ipsl.upmc.fr; cyril.lathuiliere@locean-ipsl.upmc.fr; marina.levy@locean-ipsl.upmc.fr)